Microscopic nuclear equation of state with three-body forces and neutron star structure

M. Baldo[1], **I. Bombaci**[2], **and G.F. Burgio**[1]

[1] Dipartimento di Fisica, Universitá di Catania and I.N.F.N. Sezione di Catania, c.so Italia 57, I-95129 Catania, Italy
[2] Dipartimento di Fisica, Universitá di Pisa and I.N.F.N. Sezione di Pisa, Piazza Torricelli 2, I-56100 Pisa, Italy

Abstract. We calculate static properties of non-rotating neutron stars (NS's) using a microscopic equation of state (EOS) for asymmetric nuclear matter, derived from the Brueckner-Bethe-Goldstone many-body theory with explicit three-body forces. We use the Argonne AV14 and the Paris two-body nuclear force, implemented by the Urbana model for the three-body force. We obtain a maximum mass configuration with $M_{max} = 1.8 M_\odot$ ($M_{max} = 1.94 M_\odot$) when the AV14 (Paris) interaction is used. They are both consistent with the observed range of NS masses. The onset of direct Urca processes occurs at densities $n \geq 0.65\ fm^{-3}$ for the AV14 potential and $n \geq 0.54\ fm^{-3}$ for the Paris potential. Therefore, NS's with masses above $M^{Urca} = 1.4 M_\odot$ for the AV14 and $M^{Urca} = 1.24 M_\odot$ for the Paris potential can undergo very rapid cooling, depending on the strength of superfluidity in the interior of the NS. The comparison with other microscopic models for the EOS shows noticeable differences.

Key words: dense matter – equation of state – stars: neutron

1. Introduction

In the next few years it is expected that a large amount of novel informations on neutron stars (NS's) will be available from the new generation of X-ray and γ-ray satellites. Therefore, a great interest is devoted presently to the study of NS's and to the prediction of their structure on the basis of the properties of dense matter. The equation of state (EOS) of NS matter covers a wide density range, from ~ 10 g/cm^3 in the surface to several times nuclear matter saturation density ($\rho_0 \sim 2.8\ 10^{14}$ g/cm^3) in the center of the star (Shapiro et al. 1983). The interior part (core) of a NS is made by asymmetric nuclear matter with a certain lepton fraction. At ultra-high density, matter might suffer a transition to other exotic hadronic components (like hyperons, a K^- condensate or a deconfined phase of quark matter). The possible appearance of such an exotic core has enormous consequences for the neutron star and black hole formation mechanism (Bombaci 1996). Unfortunately large uncertainties are still present in the theoretical treatment of this ultra-dense regime (Glendenning 1985, Prakash et al. 1997). Therefore, in the present work, we consider a more conventional picture assuming the NS core is composed only by an uncharged mixture of neutrons, protons, electrons and muons in equilibrium with respect to the weak interaction (β-stable matter). Even in this picture, the determination of the EOS of asymmetric nuclear matter to describe the core of the NS, remains a formidable theoretical problem (Hjorth-Jensen et al. 1995).

Any "realistic" EOS must satisfy several requirements : i) It must display the correct saturation point for symmetric nuclear matter (SNM); ii) it must give a symmetry energy compatible with nuclear phenomenology and well behaved at high densities; iii) for SNM the incompressibility at saturation must be compatible with the values extracted from phenomenology (Myers et al. 1996); iv) both for neutron matter (NEM) and SNM the speed of sound must not exceed the speed of light (causality condition), at least up to the relevant densities; the latter condition is automatically satisfied only in fully relativistic theory.

In this work we present results for some NS properties obtained on the basis of a microscopic EOS which satisfies requirements i-iv, and compare them with the predictions of other microscopic EOS's.

2. Equation of state

2.1. Brueckner-Bethe-Goldstone theory

The Brueckner-Bethe-Goldstone (BBG) theory is based on a linked cluster expansion of the energy per nucleon of nuclear matter (see *e.g.* Bethe 1971). The basic ingredient in this many-body approach is the Brueckner reaction matrix G, which is the solution of the Bethe-Goldstone equation

$$G(n;\omega) = v + v \sum_{k_a k_b} \frac{|k_a k_b\rangle Q \langle k_a k_b|}{\omega - e(k_a) - e(k_b)} G(n;\omega), \qquad (1)$$

where v is the bare nucleon-nucleon (NN) interaction, n is the nucleon number density, and ω the starting energy. The opera-

tor $|k_a k_b\rangle Q \langle k_a k_b|$ projects on intermediate scattering states in which both nucleons are above the Fermi sea (Pauli operator).

$$e(k) = e(k; n) = \frac{\hbar^2}{2m} k^2 + U(k; n) \qquad (2)$$

is the single particle energy. The Brueckner-Hartree-Fock (BHF) approximation for the s.p. potential $U(k; n)$ using the *continuous choice* is

$$U(k; n) = \sum_{k' \leq k_F} \langle kk' | G(n; e(k) + e(k')) | kk' \rangle_a \qquad (3)$$

where the subscript "a" indicates antisymmetrization of the matrix element. In this approach Eqs. (1)-(3) have to be solved self-consistently. In the BHF approximation the energy per nucleon is:

$$\frac{E}{A} = \frac{3}{5} \frac{\hbar^2}{2m} k_F^2 + D_{BHF} , \qquad (4)$$

$$D_{BHF}(n) = \frac{1}{2} \frac{1}{A} \sum_{k, k' \leq k_F} \langle kk' | G(n; e(k) + e(k')) | kk' \rangle_a \qquad (5)$$

In this scheme, the only input quantity we need is the bare NN interaction v in the Bethe-Goldstone equation (1). In this sense the BBG approach can be considered as a microscopic one.

The Brueckner-Hartree-Fock (BHF) approximation for the EOS in SNM, within the continuous choice (Baldo et al. 1991), reproduces closely results which include up to four hole line diagram contributions to the BBG expansion of the energy, calculated within the so called *gap choice* for the single particle potential $U(k)$ (Day et al. 1985). In the following we refer to the latter calculations as BBG_4^{gap}. The numerical accuracy of the solution of the BHF equation in the continuous choice has been discussed recently in ref. (Schulze et al. 1995).

In Fig. 1 we show the energy per nucleon calculated within this scheme in the case of SNM (lower curves) and NEM (upper curves); the solid and dashed curves have been obtained using respectively the Paris potential (Lacombe et al. 1980) and the Argonne v_{14} (AV14) model (Wiringa et al. 1984) for the two-body nuclear force. For comparison, we report in the same figure the energy per nucleon calculated within the variational many-body approach (Wiringa et al. 1988, hereafter WFF) using respectively the AV14 (open circles) and the Urbana UV14 (squares) two-nucleon potentials.

We notice that both the BHF and the variational approach fail to reproduce the empirical saturation point of nuclear matter ($n_o = 0.17 \pm 0.01$ fm^{-3}, $E_o/A = -16 \pm 1$ MeV). Analogous non-relativistic calculations have been performed with the Bonn potential (Machleidt 1989, Engvik et al. 1996). Even in that case symmetric nuclear matter does not saturate at the empirical point.

The comparison of the saturation curves obtained in the BHF and the variational approach with the same two-nucleon AV14 potential shows that our BHF saturation point ($n_o = 0.256$ fm^{-3}, $E_o/A = -18.26$ MeV) is closer to the empirical saturation point than the one reported in WFF paper
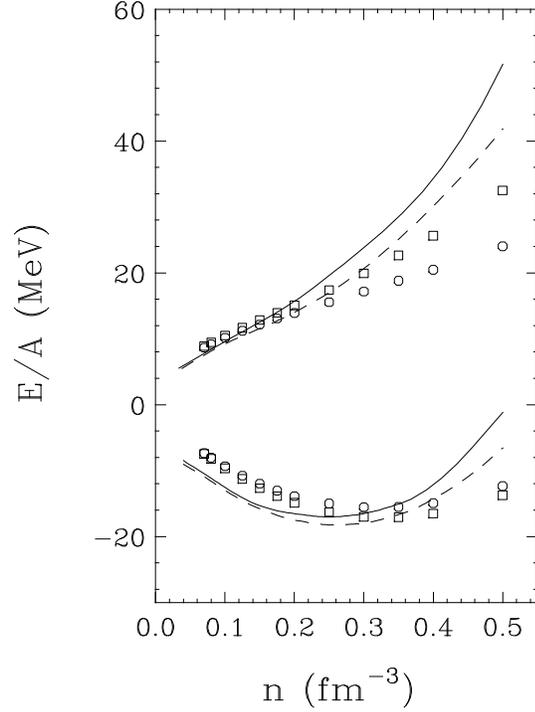

Fig. 1. The energy per baryon E/A is plotted vs. the number density n for symmetric matter (lower curves) and for neutron matter (upper curves). The solid (dashed) line represents a non-relativistic Brueckner calculation with Paris (AV14) potential, whereas the open circles (squares) are the results of a variational calculation performed with AV14 (UV14) interaction.

($n_o = 0.319$ fm^{-3}, $E_o/A = -15.6$ MeV). The two methods give results in reasonable agreement in the case of SNM up to a density $n \simeq 0.4$ fm^{-3}, whereas sizeable differences are evident for NEM already at densities $n \simeq 0.3$ fm^{-3}. A similar outcome has been found by comparing variational and BBG_4^{gap} saturation curves for the same NN potential (Day, et al 1985). The discrepancy clearly arises from the different many-body technique.

In Fig. 2 we report the energy per nucleon as a function of the number density n calculated in the BHF approximation using the Paris (solid curves) and the AV14 potentials (dashed curves) up to densities typically encountered in the core of a neutron star. The upper curves refer to neutron matter and the lower ones to symmetric nuclear matter. We notice that the EOS derived with the Paris potential is stiffer than the one obtained with the AV14 interaction. This is possibly due to the momentum dependence of the Paris potential, as discussed recently in ref.(Engvik et al. 1997).

2.2. Three-body forces

Non-relativistic calculations, based on purely two-body interactions, fail to reproduce the correct saturation point for symmetric nuclear matter (Coester et al. 1970). This well known deficiency is commonly corrected introducing three-body forces
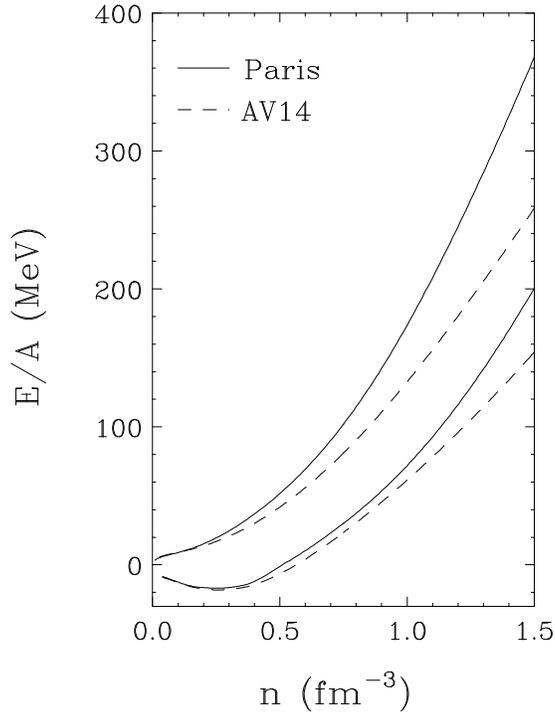
Fig. 2. The energy per baryon E/A is plotted vs. the number density n for symmetric matter (lower curves) and for neutron matter (upper curves). Non-relativistic Brueckner calculations are drawn for the AV14 (dashed line) and the Paris (solid line) potentials.

(TBF). Unfortunately, it seems not possible to reproduce the experimental binding energies of light nuclei and the correct saturation point accurately with one simple set of TBF (Wiringa et al. 1988). Relevant progress has been made in the theory of nucleon TBF, but a complete theory is not yet available. A realistic model for nuclear TBF has been introduced by the Urbana group (Carlson et al. 1983; Schiavilla et al. 1986). The Urbana model consists of an attractive term $V_{ijk}^{2\pi}$ due to two-pion exchange with excitation of an intermediate Δ-resonance, and a repulsive phenomenological central term V_{ijk}^R

$$V_{ijk} = V_{ijk}^{2\pi} + V_{ijk}^R \tag{6}$$

The two-pion exchange contribution is a cyclic sum over the nucleon indices *i, j, k* of products of anticommutator {,} and commutator [,] terms

$$V_{ijk}^{2\pi} = A \sum_{cyc} \left(\{X_{ij}, X_{jk}\}\{\tau_i \cdot \tau_j, \tau_j \cdot \tau_k\} \right. \tag{7}$$

$$\left. + \frac{1}{4}[X_{ij}, X_{jk}][\tau_i \cdot \tau_j, \tau_j \cdot \tau_k] \right), \tag{8}$$

where

$$X_{ij} = Y(r_{ij})\sigma_i \cdot \sigma_j + T(r_{ij})S_{ij} \tag{9}$$

is the one-pion exchange operator, σ and τ are the Pauli spin and isospin operators, and $S_{ij} = 3\left[(\sigma_i \cdot r_{ij})(\sigma_j \cdot r_{ij}) - \sigma_i\sigma_j\right]$

is the tensor operator. $Y(r)$ and $T(r)$ are the Yukawa and tensor functions, respectively, associated to the one-pion exchange, as in the two-body potential.

The repulsive part is taken as

$$V_{ijk}^R = U \sum_{cyc} T^2(r_{ij})T^2(r_{jk}) \tag{10}$$

The constants A and U in the previous equations can be adjusted to reproduce observed nuclear properties. Within this scheme Schiavilla *et al.* (1986) found $A = -0.0333$ and $U = 0.0038$ by fitting properties of light nuclei (^{3}H, ^{4}He), the so called Urbana VII parametrization (UVII) (Carlson et al. 1983).

We introduced the same Urbana three-nucleon model within the BHF approach. To incorporate the TBF in the Brueckner scheme we followed the method of Lejeune et al. (1986). The TBF is reduced to an effective two-body force by averaging on the position of the third particle, assuming that the probability of having two particles at a given distance is reduced according to the two-body correlation function. The resulting effective two-body force is of course density dependent. Further details will be given elsewhere (Baldo et al. in preparation). We have adjusted the parameters A and U in order to reproduce closely the correct saturation point of SNM, since for NS studies this is an essential requirement, and there is no reason to believe that TBF be the same as in light nuclei. Our values for the TBF parameters are $A' = -0.0329$ and $U' = 0.00361$ both for the Paris and the AV14 potentials.

The corresponding EOS's obtained using the Paris (solid line) and the AV14 potentials (short dashed line) are depicted in Fig. 3 for symmetric (panel (a)) and neutron matter (panel (b)). The corresponding values are reported in Table 1. Those EOS's saturate respectively at

$$n_o = 0.176 \ fm^{-3}, \quad E_o/A = -16.01 \ MeV \quad Paris \tag{11}$$

and

$$n_o = 0.178 \ fm^{-3}, \quad E_o/A = -16.46 \ MeV \quad AV14 \tag{12}$$

They are characterized by an incompressibility $K_\infty^{Paris} = 281 \ MeV$ and $K_\infty^{AV14} = 253 \ MeV$, the latter being very close to the recent phenomenological estimate of Myers (1996). In the same figure, we show the EOS obtained within the variational many-body approach by WFF when the UVII parametrization (Carlson et al. 1983, Schiavilla et al. 1986) is added to the AV14 two-body force (open circles).

We have already noticed that both the BHF and the variational many-body methods produce a different saturation point already at the two-body level. As a consequence, the values of the strengths (A' and U') of the attractive and repulsive TBF needed to reproduce empirical saturation are different with respect to those used by WFF in their work. In particular, being $U' < U$, our repulsive TBF is weaker. Consequently, our EOS's are softer than the WFF at very high density (see Fig. 3) where the repulsive component of the TBF is dominant.

In Fig. 3 we plot also the EOS from a recent Dirac-Brueckner calculation (DBHF) (Li et al. 1992) with the Bonn-A
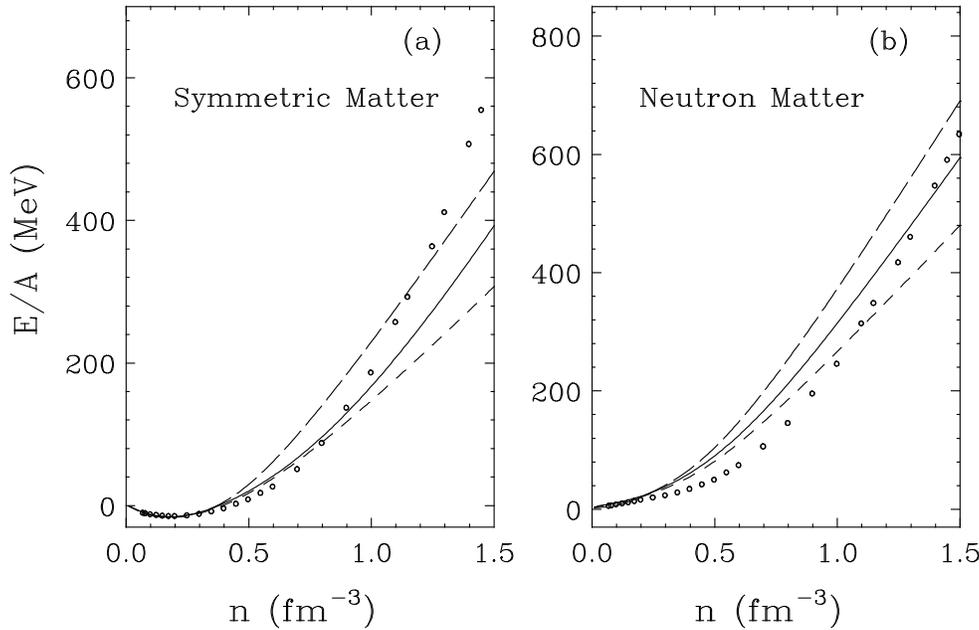
Fig. 3a and b. The energy per baryon E/A is plotted vs. the number density n for symmetric matter (panel **a**) and for neutron matter (panel **b**). Several EOS's are shown, i.e. non-relativistic Brueckner calculations with three-body forces (solid line, Paris potential; short dashed line, AV14 potential) and a relativistic Dirac-Brueckner one (long dashes, DBHF). For comparison a variational calculation (with AV14+UVII interaction) is also reported (open circles, WFF).

Table 1. The energy per baryon E/A in MeV is shown vs. the number density n in fm^{-3} for symmetric matter and neutron matter. The values are the results of a non-relativistic BHF calculation with AV14 and Paris potentials with three-body forces.

n	$AV14 + TBF_{sym}$	$Paris + TBF_{sym}$	$AV14 + TBF_{neu}$	$Paris + TBF_{neu}$
0.08	-11.47	-10.8	8.54	9.47
0.16	-16.32	-15.88	16.2	17.
0.2	-16.25	-15.74	21.	22.1
0.3	-10.78	-9.4	35.6	38.8
0.4	0.79	3.2	55.26	61.4
0.5	17.53	20.46	81.13	90.3
0.6	38.5	41.78	112.5	125.55
0.7	62.7	67.17	147.9	166.7
0.8	89.3	96.7	185.9	212.66
0.9	117.67	130.22	225.7	262.3
1.	147.35	167.4	266.7	314.6
1.1	178.	207.76	308.4	368.78
1.2	209.5	250.87	350.8	424.12
1.3	241.58	296.27	393.5	480.3
1.4	274.17	343.6	436.6	537.
1.5	307.18	392.52	479.8	594.2

two-body force (long dashed line). In the low density region ($n < 0.4 \ fm^{-3}$), both BHF equations of state with TBF and DBHF equations of state are very similar, whereas at higher density the DBHF is stiffer. The discrepancy between the non-relativistic and relativistic calculation of the EOS can be easily understood by noticing that the DBHF treatment is equivalent (Baldo et al. 1995) to introduce in the non-relativistic BHF the three-body force corresponding to the excitation of a nucleon-antinucleon pair, the so-called Z-diagram (Brown et al. 1987). The latter is repulsive at all densities. In BHF treatment, on the contrary, both attractive and repulsive three-body forces are introduced, and therefore a softer EOS can be expected. It should be noticed that, because of the strong repulsion at short distances, our BHF calculation with three-body force is numerically stable up to densities $n \simeq 0.8 \ fm^{-3}$. Moreover, the relativistic DBHF calculations are available in literature up to densities $n = 0.75 \ fm^{-3}$ (Li et al., 1992). Since the typical densities encountered in the core of neutron stars are larger, both microscopic calculations need to be either extrapolated to slightly higher densities or joined with other high density equations of state, several of which are available in literature. We decided to perform a numerical extrapolation to the needed higher densities. In the extrapolation procedure we keep checking that the *causality condition* is fulfilled, i.e.

$$c_s/c \equiv \left(\frac{dP}{d\varepsilon}\right)^{1/2} \leq 1, \tag{13}$$
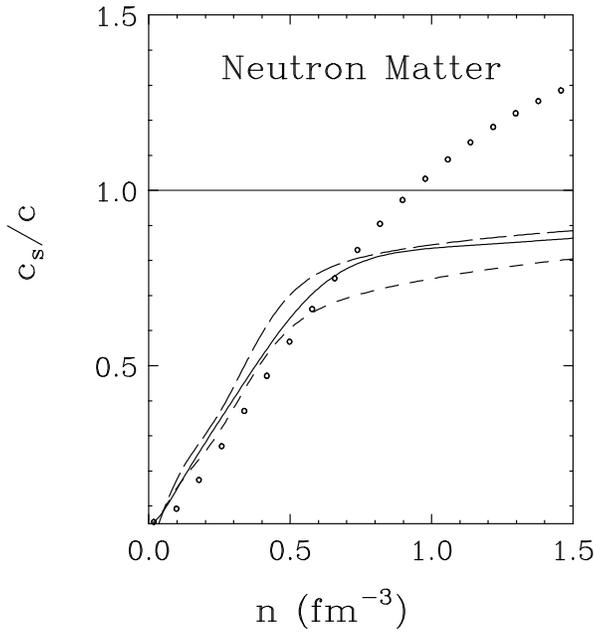
Fig. 4. The ratio c_s/c is plotted as a function of the number density for pure neutron matter. The notation is the same as in Fig. 3.

which means that the speed of sound c_s in matter must be lower than the speed of light in the vacuum. This is a basic trait of any "realistic" EOS, regardless the details of the interactions among matter constituents or the many-body approach. Details on the extrapolation procedure are given in Sect. 3.

The ratio c_s/c as a function of the number density is reported in Fig. 4, in the case of pure neutron matter, for our BHF models (AV14 + TBF(short dashes), Paris + TBF (solid)), and the DBHF model (long dashes). WFF model (open circles) violates the causality condition at densities encountered in the core of neutron stars near the maximum mass configuration predicted by that model (Wiringa et al.,1988).

2.3. Symmetry energy and EOS for β-stable matter

The energy per nucleon of asymmetric nuclear matter ($n_n \neq n_p$, being n_n and n_p the neutron and proton number densities respectively) can be calculated extending the original BBG theory for SNM sketched in Sect. 2.1. (Bombaci et al. 1994). From the energy per nucleon one defines the nuclear symmetry energy as

$$E_{sym}(n) \equiv \frac{1}{2} \frac{\partial^2 E/A}{\partial \beta^2}\bigg|_{\beta=0} \qquad (14)$$

where we introduce the *asymmetry parameter*

$$\beta = \frac{n_n - n_p}{n}, \qquad (15)$$

with $n = n_n + n_p$. At the saturation density, $E_{sym}(n_o)$ corresponds to the symmetry coefficient in the Weizsäcker-Bethe semiempirical mass formula, and its value extracted from nuclear systematics lies in the range 28-32 MeV.

In the present work, we calculate the energy per nucleon of asymmetric nuclear matter assuming the so called *parabolic approximation*

$$\frac{E}{A}(n, \beta) = \frac{E}{A}(n, \beta = 0) + E_{sym}(n)\beta^2, \qquad (16)$$

In this approximation the symmetry energy can be expressed in terms of the difference of the energy per particle between neutron ($\beta = 1$) and symmetric ($\beta = 0$) matter:

$$E_{sym}(n) = \frac{E}{A}(n, \beta = 1) - \frac{E}{A}(n, \beta = 0) \qquad (17)$$

The reliability of the parabolic approximation has been checked microscopically by Bombaci and Lombardo (1991). Then we determine the composition of β-stable matter, at a given nucleon number density, solving the equations for chemical equilibrum (for neutrino-free matter, $\mu_{\nu_e} = \mu_{\nu_\mu} = 0$)

$$\mu_e = \mu_n - \mu_p \equiv \hat{\mu} \qquad (18)$$

$$\mu_e = \mu_\mu \qquad (19)$$

and charge neutrality

$$n_p = n_e + n_\mu, \qquad (20)$$

being μ_i ($i = n, p, e, \mu$) the chemical potentials of star constituents. Therefore, in the case of neutrino-free matter, the leptonic chemical potential is determined once the difference $\hat{\mu} \equiv \mu_n - \mu_p$ is known. The latter quantity can be expressed as:

$$\hat{\mu} = -\frac{\partial E/A}{\partial x}\bigg|_n = 2\frac{\partial E/A}{\partial \beta}\bigg|_n \qquad (21)$$

where $x = n_p/n = (1-\beta)/2$ is the proton fraction and the partial derivatives are taken for constant nucleon number density n. In Eq. (21) we neglect the neutron-proton mass difference.

In the parabolic approximation (16) for the energy per nucleon of asymmetric nuclear matter one has

$$\hat{\mu} = 4E_{sym}(n)(1 - 2x) \qquad (22)$$

Therefore the composition of β-stable matter, and in particular the proton fraction x, is strongly dependent on the nuclear symmetry energy.

As it has been recently pointed out by Lattimer et al. (1991), the value of the proton fraction in the core of NS is crucial for the onset of direct Urca processes, whose occurrence enhances neutron star cooling rates.

The values of E_{sym} for the different EOS's are reported in Fig. 5 (panel (a)), together with the corresponding proton fraction (panel (b)). The long dashed line represents the relativistic DBHF calculation[1], whereas the non-relativistic Brueckner calculations with the AV14 + TBF and the Paris + TBF models are

---

[1]   In a recent paper (Lee et al., 1997) the authors show microscopic calculations of asymmetric nuclear matter in the DBHF approach up to densities $n = 1.1\ fm^{-3}$. They obtain a symmetry energy which saturates with increasing density, at variance with our findings. In spite of that the values of the maximum mass configuration are similar to those calculated in this work.
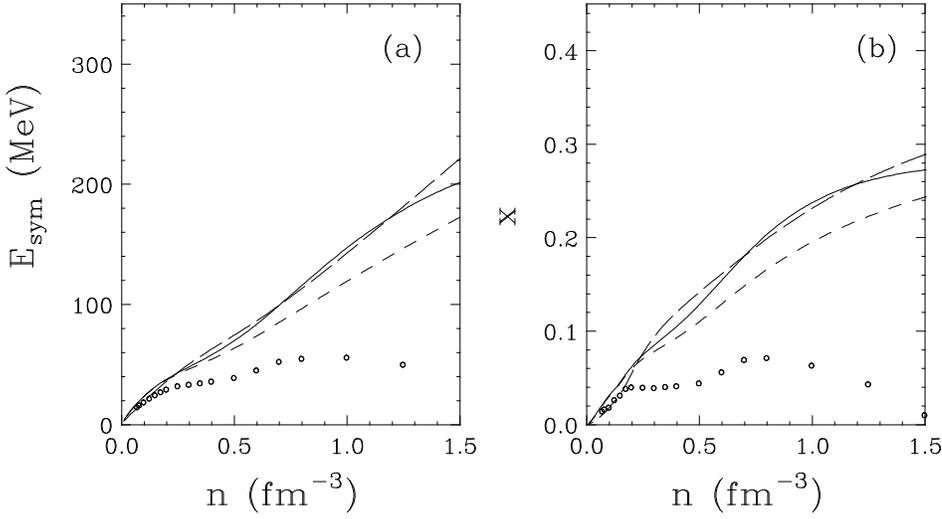
Fig. 5a and b. The symmetry energy and the proton fraction are shown vs. number density respectively in panel **a** and **b**. The notation is the same as in Fig. 3.
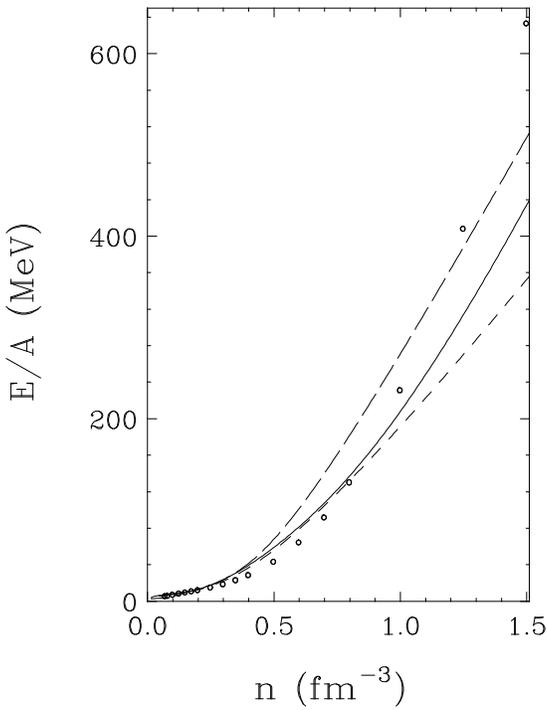

Fig. 6. The energy per baryon E/A of asymmetric nuclear matter in β-equilibrium (with electrons and muons) is plotted vs. the number density n. Different curves are denoted as in Fig. 3.

respectively represented by a short dashed and a solid line. We notice that in both relativistic and non-relativistic Brueckner-type calculations, the proton fraction x can exceed the "critical" value $x^{Urca} = (11 - 15)\%$ needed for the occurrence of direct Urca processes (Lattimer et al. 1991). This is at variance with the WFF variational calculation (open circles), which predicts a low absolute value both for the symmetry energy and the proton fraction with a slight bend over. For the AV14 + TBF model we find $x^{Urca} = 13.9\%$, which correspond to a critical density

$n^{Urca} = 0.65 \; fm^{-3}$, whereas the Paris + TBF model predicts the same critical proton fraction at density $n^{Urca} = 0.54 \; fm^{-3}$. Therefore, BHF neutron stars with a central density higher than n^{Urca} develop inner cores in which direct Urca processes are allowed.

In Fig. 6, we show the energy per baryon of asymmetric nuclear matter in β-equilibrium, for the models under consideration. We notice that the AV14 and the Paris two-nucleon interactions, implemented by the same three-body force, produce similar EOS's up to densities $n \simeq 0.8 \; fm^{-3}$, whereas the high density region is quite different. Therefore we find the same trend as observed in Fig. 2.

From the energy per baryon of asymmetric nuclear matter in β-equilibrium, we calculate the nuclear contribution P_{nucl} to the total pressure of stellar matter using the thermodynamical relation

$$P_{nucl}(n) = n^2 \frac{d \, (E/A)}{dn}\bigg|_A \tag{23}$$

Then the total pressure and total mass density ρ are given by

$$P = P_{nucl} + P_{lep} \tag{24}$$

$$\rho = \frac{1}{c^2}\left(\varepsilon_{nucl} + \varepsilon_{lep}\right) = \frac{1}{c^2}\left(n \, E/A + n \, m_N + \varepsilon_{lep}\right) \tag{25}$$

being P_{lep} and ε_{lep} the leptonic contributions to the total pressure and energy density, m_N the nucleon mass and c the speed of light in the vacuum.

Our EOS's for β-stable matter (neutrons, protons, electrons and muons) calculated with AV14 (Paris) potential plus Urbana three-body forces are given respectively in Table 2 (3).

3. Neutron star structure

The EOS for β-stable matter can be used in the Tolman-Oppenheimer-Volkoff (Tolman 1934, Oppenheimer et al. 1939) equations to compute the neutron star mass and radius as a function of the central density.
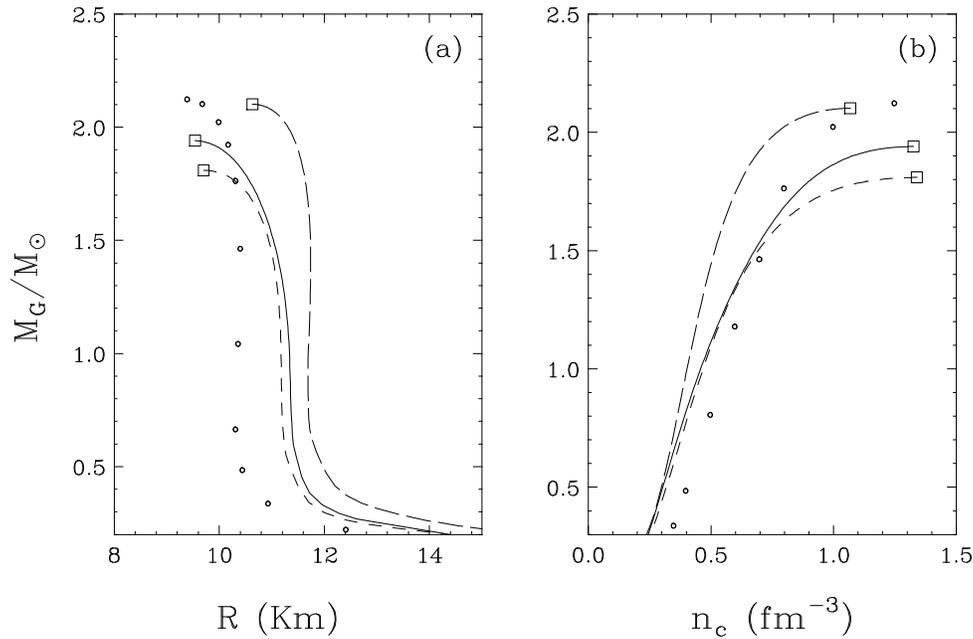
Fig. 7a and b. The gravitational mass M_G, expressed in units of the solar mass $M_\odot$, is displayed vs. radius R (panel **a**) and the central number density n_c (panel **b**). The notation is the same as in Fig. 3. The squares represent the values of the limiting configuration.

Table 2. EOS for β-stable matter obtained in BHF approximation using the Argonne AV14 two-body interaction implemented by TBF as described in the text. We display the number density n in units of fm^{-3}, the proton fraction x, the total mass density ρ and the total pressure P.

n	x	ρ (10^{14} $g\ cm^{-3}$)	P (10^{34} $dyn\ cm^{-2}$)
0.08	0.025	1.35	0.042
0.16	0.048	2.7	0.244
0.2	0.06	3.4	0.502
0.3	0.078	5.15	1.88
0.4	0.093	6.98	4.62
0.5	0.11	8.92	8.92
0.6	0.129	10.97	14.7
0.7	0.148	13.13	21.87
0.8	0.166	15.42	30.36
0.9	0.182	17.85	40.14
1.	0.195	20.39	51.19
1.1	0.207	23.07	63.5
1.2	0.218	25.88	77.04
1.3	0.227	28.82	91.8
1.4	0.236	31.88	107.78
1.5	0.243	35.07	124.96

Table 3. Same as Table 2, but for Paris potential as NN interaction.

n	x	ρ (10^{14} $g\ cm^{-3}$)	P (10^{34} $dyn\ cm^{-2}$)
0.08	0.025	1.35	0.039
0.16	0.05	2.7	0.243
0.2	0.062	3.4	0.53
0.3	0.085	5.17	2.07
0.4	0.105	7.	4.83
0.5	0.128	8.95	8.95
0.6	0.155	11.0	14.8
0.7	0.18	13.2	23.
0.8	0.204	15.55	34.
0.9	0.223	18.06	48.
1.	0.237	20.77	64.9
1.1	0.25	23.67	84.53
1.2	0.257	26.78	106.6
1.3	0.264	30.1	131.
1.4	0.269	33.6	157.6
1.5	0.272	37.3	186.4

We assume that a neutron star is a spherically symmetric distribution of mass in hydrostatic equilibrium. We neglect the effects of rotations and magnetic fields. Then the equilibrium configurations are simply obtained by solving the Tolman-Oppenheimer-Volkoff (TOV) equations for the total pressure P and the enclosed mass m,

$$\frac{dP(r)}{dr} = -\frac{Gm(r)\rho(r)}{r^2}\frac{(1+\frac{P(r)}{c^2\rho(r)})(1+\frac{4\pi r^3 P(r)}{c^2 m(r)})}{(1-\frac{2Gm(r)}{rc^2})} \tag{26}$$

$$\frac{dm(r)}{dr} = 4\pi r^2 \rho(r) \tag{27}$$

being G the gravitational constant. Starting with a central mass density $\rho(r=0) \equiv \rho_c$, we integrate out until the pressure on the surface equals the one corresponding to the density of iron. This gives the stellar radius R and the gravitational mass is then

$$M_G \equiv m(R) = 4\pi \int_0^R dr\ r^2 \rho(r). \tag{28}$$

For the outer part of the neutron star we have used the equations of state by Feynman-Metropolis-Teller (Feynman et al. 1949) and Baym-Pethick-Sutherland (Baym et al. 1971), and for the middle-density regime (0.001 $fm^{-3} < n < 0.08\ fm^{-3}$) we use the results of Negele and Vautherin (Negele et al. 1973). In the high-density part ($n > 0.08\ fm^{-3}$) we use alternatively the four EOS's discussed above. The results are reported in Fig. 7.

Table 4. Properties of the maximum mass configuration obtained for different equations of state: M_G is the gravitational (maximum) mass, R is the corresponding radius, n_c the central number density and x_c the central proton fraction.

EOS	$M_G/M_\odot$	R(km)	$n_c(fm^{-3})$	x_c
AV14	1.5	8.1	1.9	0.17
Paris	1.66	8.	1.88	0.26
AV14 + TBF	1.8	9.7	1.34	0.23
Paris + TBF	1.94	9.54	1.33	0.265
DBHF	2.1	10.6	1.07	0.24
WFF	2.130	9.40	1.25	0.045

Table 5. Properties of neutron stars with $M_G = 1.4\ M_\odot$

EOS	R(km)	$n_c(fm^{-3})$	x_c
AV14	8.92	1.27	0.12
Paris	9.3	1.08	0.178
AV14 + TBF	11.	0.65	0.139
Paris + TBF	11.09	0.64	0.165
DBHF	11.74	0.49	0.14
WFF	10.41	0.66	0.0658

We display the gravitational mass M_G, in units of the solar mass $M_\odot$ ($M_\odot = 1.99\ 10^{33}$ g), as a function of the radius R (panel (a)) and the central number density n_c (panel (b)). The notation is the same as in the previous figures.

As expected, the stiffest EOS within the Brueckner scheme (DBHF) we used in the present calculation gives higher maximum mass and lower central density with respect to the non-relativistic Brueckner models.

The properties of the maximum mass configuration, for each EOS, are summarized in Table 4, whereas in Table 5 the properties of neutron stars with gravitational mass $M_G = 1.4\ M_\odot$ are reported. However, the properties of each configuration extracted by solving the TOV equations are slightly dependent on the extrapolation parameters we used. This holds for the DBHF equation of state and the Paris + TBF model, while in the case of Argonne AV14 + TBF model no seizable dependence was found. For the BHF calculation with only two-body forces no extrapolation is needed. In any case the dependence on the extrapolation procedure turns out to be rather weak. We have used a fractional polynomial extrapolation of the form

$$\frac{E}{A} = \frac{Q^\sigma(n)}{1 + b\ n^\sigma} \tag{29}$$

where the coefficients of the polynomial Q are fitted to reproduce the EOS up to the maximum calculated density n, and the coefficient b ensures that for very large values of n the energy per baryon does not diverge. Different values for the polynomial degree σ can be used and different extrapolated EOS are in general obtained. However we found that the critical mass, radius and central densities do not vary more than 5% with $\sigma = 3,\ 4$ and b ranging from 10^{-2} to 10^{-3} for the case of the Paris potential + TBF model calculations, while in all other cases the variations can be considered negligeable.

As one can see from Table 4, the values of the limiting mass configuration are strongly modified by the presence of the nuclear TBF in the equation of state, in particular by their repulsive contribution which dominates at high densities. However, the non-relativistic BHF calculations implemented by three-body force do not strongly depend on the two-body interaction, and predict very close limiting values of the maximum mass (within the numerical uncertainties due to the extrapolation).

The difference between BHF and WFF neutron stars reflects the discrepancy already noticed for the EOS and mainly for the symmetry energy. This point will be discussed in more details in a forthcoming paper (Baldo et al., in preparation).

Our calculated BHF configurations with three-body forces are consistent with the measured masses of X-ray pulsars and radio pulsars (van Kerkwijk et al. 1995).

4. Conclusions

In conclusion, we computed some properties of NS's on the basis of a microscopic EOS obtained in the framework of BBG many-body theory with two- and three-body nuclear interactions. Our Brueckner-Hartree-Fock EOS with three-body forces satisfies the general physical requirements (points i-iv) discussed in the introduction. This is the main feature which distinguishes our EOS's with respect to other microscopic non-relativistic EOS (Wiringa et al. 1988, Engvik et al. 1994, 1996). Two different two-body potentials have been used, the Argonne AV14 and the Paris interactions. The latter turns out to produce a slightly stiffer EOS already at two-body level. The same three-body force, within the Urbana model, has been added to both two-body interactions, and this produces similar saturation points close to the empirical one. The BHF calculations with three-body forces show again that the Paris potential gives an EOS stiffer than the one from the Argonne AV14 and a larger symmetry energy as a function of density. As a consequence the proton fraction is larger for the Paris and the Urca process onset appears at lower density.

The calculated maximum mass is in agreement with observed NS masses (van Kerkwijk et al. 1995). However the limiting mass, radius and central density are relatively close to each other for the two interactions. In particular the critical masses differ by no more than 8%, while the radius and central density are essentially equal. On the contrary all these three critical physical parameters are appreciably different from the ones derived from the Dirac-Brueckner approach (Li et al. 1992) as well as from the variational results. The latter displays also a rather different trend of the symmetry energy.

For the Argonne AV14 (Paris) potential the BHF approach with three-body forces predicts a lower limit for the mass above which neutron stars can support the direct Urca process, $M^{Urca} = 1.4 M_\odot$ ($1.24 M_\odot$). The stars with mass larger than this value cool very rapidly or not depending on the properties of nuclear superluidity (values of the superfluid gaps, critical temperatures, density ranges for the superfluid transition)(Page et al. 1992, Baldo et al. 1995). The EOS's developed in this paper offer the possibility for a selfconsistent microscopic calculation

for both the neutron star structure, and nuclear superfluid properties within the same many-body approach and with the same nuclear interaction.

References

Baldo M., Bombaci I., Ferreira L.S., Giansiracusa G. and Lombardo U., 1991, Phys. Rev. C43, 2605 and references therein

Baldo M., Giansiracusa G., Lombardo U., Bombaci I. and Ferreira L.S., 1995, Nucl. Phys. A583, 599

Baldo M., Lombardo U., Bombaci I. and Schuck P., 1995, Phys. Rep. 242, 159 and references therein

Baldo M., Bombaci I., Burgio G.F. and Giambrone G., in preparation

Baym G., Pethick C. and Sutherland D., 1971, ApJ 170, 299

Bethe H.A., 1971, Ann. Rev. Nucl. Sci. 21, 93

Bombaci I., 1996, A&A 305, 871

Bombaci I. and Lombardo U., 1991, Phys. Rev. C44, 1892

Bombaci I., Kuo T.T.S. and Lombardo U., 1994, Phys. Rep. 242, 165

Brown G.E., Weise W., Baym G. and Speth J., 1987, Comm. Nucl. Part. Phys. 17, 39

Carlson J., Pandharipande V.R. and Wiringa R.B., 1983, Nucl. Phys. A401, 59

Coester F., Cohen S., Day B.D., and Vincent C.M., 1970, Phys. Rev. C1, 769

Day B.D. and Wiringa R.B., 1985, Phys. Rev. C32, 1057

Engvik L., Osnes E., Hjorth-Jensen M., Bao G. and Ostgaard E., 1996, ApJ 469, 794; 1994, Phys. Rev. Lett. 73, 2650

Engvik L., Hjorth-Jensen M., Machleidt R., Müther H. and Polls A., 1997, " Non-local vs. local nucleon-nucleon potentials: consequences for neutron star properties", submitted to Nuclear Physics A.

Feynman R., Metropolis F. and Teller E., 1949, Phys. Rev. 75, 1561

Glendenning N.K., 1985, ApJ 293, 470

Hjorth-Jensen M., Kuo T.T.S. and Osnes E., 1995, Phys. Rep. 261, 125

Lacombe M., Loiseau B., Richard J.M., Vinh Mau R., Còté J., Pirés P. and de Tourreil R., 1980, Phys. Rev. C21, 861

Lattimer J., Pethick C., Prakash M. and Haensel P., 1991, Phys. Rev. Lett. 66, 2701

Lee C.H., Kuo T.T.S., Li G.Q. and Brown G.E., "Symmetry Energy of Nuclear Matter and Properties of Neutron Stars in a relativistic Approach", preprint SUNY-NTG-97-10

Lejeune A., Grangé P., Martzolff M. and Cugnon J., 1986, Nucl. Phys. A453, 189

Li G.Q., Machleidt R. and Brockmann R., 1992, Phys. Rev. C45, 2782

Machleidt R., 1989, Adv. Nucl. Phys. 19, 189

Myers W.D. and Swiatecky W.J., 1996, Nucl. Phys. A601, 141

Negele J.W. and Vautherin D., 1973, Nucl. Phys. A207, 298

Oppenheimer J. and Volkoff G., 1939, Phys. Rev. 55, 374

Page D. and Applegate J.H., 1992, ApJ 394, L17

Prakash M., Bombaci I., Prakash M. et al., 1997, Phys. Rep. 280, 1

Schiavilla R., Pandharipande V.R. and Wiringa R.B., 1986, Nucl. Phys. A449, 219

Schulze H.-J., Cugnon J., Lejeune A., Baldo M. and Lombardo U., 1995, Phys. Rev. C52, 2785

Shapiro S. and Teukolsky S., "Black Holes, White Dwarfs and Neutron Stars", (John Wiley & Sons 1983) USA

Tolman R.C., 1934, Proc. Nat. Acad. Sci. USA 20, 3

van Kerkwijk M.H., van Paradijs J. and Zuiderwijk E.J., 1995, A&A 303, 497

Wiringa R.B., Smith R.A. and Ainsworth T.L., 1984, Phys. Rev. C29, 1207

Wiringa R.B., Fiks V. and Fabrocini A., 1988, Phys. Rev. C38, 1010